Simulations of two-phase kerosene/air rotating detonation engine at Ma5 flight conditions

Fang Wang*, Qiuyue Liu, Chunsheng Weng
Nanjing University of Science and Technology
Nanjing, Jiangsu, China

1 Introduction

Rotating detonation engine (RDE) is a novel engine that is based on detonation combustion[1]. The propulsion devices adopting detonation have high thermal efficiency, large specific impulse and compact structure, thereby having superiority over deflagration-based devices. RDE, essentially consisting of an annulus with one end open and the other end having a valve system, becomes the most promising pressure gain device up to now. Fuel and oxidizer enter axially through the valve end. Combustion products exit predominantly axially from the open end and therefore generate thrust. RDE has wide application prospects in addressing the thermal efficiency bottleneck, such as rocket engines, turbine engines, and ramjet engines.

Recent research demonstrates significant progress in the propagation mechanism and engineering development of the two-phase rotating detonation engines. In experiments, Wolanski et al. [2] reported the RDE experiments conducted with two different liquid fuels, extraction gasoline and Jet-A, by a new mixture preparation method of the preheated liquid fuel partially mixed with hot air. Rotating detonation waves were achieved for different equivalence ratios. Their research prepares the way for the application of RDE to turbine engines and jet propulsion systems. Our previous study[3, 4] reported the achievement of direct-connect RDE experiments in a cavity-based annular combustor to approach the Mach 4 flight condition at an altitude of 20 km. liquid kerosene was directly injected into the combustor and rotating detonation waves were observed with approximately 60% of the Chapman–Jouguet velocity. Apart from the air-breathing conditions, Heister et al. [5, 6] also explored the detonation wave structure of a rocket RDE using gas/liquid propellants. It was found that smaller droplet diameters, higher base pressures, and reactants with lower sound speeds are desired for close coupling of the leading shock front to the heat-release zone.

In addition to the experiments, simulations were also conducted on the two-phase rotating detonation waves to help understand the complex phenomenon existing therein. Zhang et al. [7] developed a two-phase detonation solver called RYrhoCentralFoam for multi-phase, multi-component, compressible and reacting flows. Their research mainly interests n-heptane/air RDE and factors such as the equivalence ratio[8], chemistry[9], and vapor/droplet concentrations[10]. Ren et al. [11] performed simulations on the two-phase kerosene/air rotating detonation and their emphasis is placed on the propagation stability of rotating detonation waves. Wang et al. [12] investigated the kerosene/air rotating detonation waves

Correspondence to: wfnjust@126.com

under different injection total temperatures and droplet sizes. The stratification of the fresh mixture layer is observed where the upper layer is mainly fuel vapor and the lower layer is mainly fuel droplets. These simulations involve large aspects of the ground operation of two-phase RDE, while research regarding the RDE operating under real flight conditions is still insufficient. Since the breakthrough has been achieved at ground operation conditions, the development direction will be placed on real flight conditions and the insight into RDE operating at the real flight condition becomes increasingly urgent.

In this paper, numerical simulations were performed on the two-phase kerosene/air rotating detonation engine operating at Mach 5 and 24 km. The engine size effects and the droplet size effects are investigated at real flight conditions. The rest of the paper is organized as follows. Firstly, the governing equations and numerical method will be presented in Section 2. Next, the results and discussion are presented in Section 3. Finally, the conclusions drawn from this work are presented in Section 4.

2 Governing equations and numerical method

2.1 Governing equations

As for the gas phase, the Navier-Stokes equations are solved for compressible, multi-component and reactive flows. The droplet volume fraction effects on the gas phase are neglected since dilute sprays are considered [13]. The equations of mass, momentum, energy and species mass fraction read

$$\frac{\partial \rho}{\partial t} + \nabla \cdot [\rho \mathbf{u}] = S_{mass}, \tag{1}$$

$$\frac{\partial (\rho \mathbf{u})}{\partial t} + \nabla \cdot [\mathbf{u} \cdot (\rho \mathbf{u})] + \nabla p + \nabla \cdot \mathbf{T} = \boldsymbol{S}_{mom,} \tag{2}$$

$$\frac{\partial (\rho \mathbf{E})}{\partial t} + \nabla \cdot [\mathbf{u}(\rho \boldsymbol{E} + \mathbf{p})] + \nabla \cdot [\mathbf{T} \cdot \mathbf{u}] + \nabla \cdot \mathbf{j} = \dot{\omega}_T + S_{energy,} \tag{3}$$

$$\frac{\partial (\rho Y_m)}{\partial t} + \nabla \cdot [\mathbf{u}(\rho Y_m)] + \nabla \cdot \mathbf{s}_m = \dot{\omega}_m + S_{species,m,} \ (m = 1, \dots M - 1), \tag{4}$$

$$p = \rho R T. \tag{5}$$

Here t is time, ρ the gas density, $\mathbf{u}$ the gas velocity vector, T the gas temperature, p the pressure, Y_m the mass fraction of m-th species, and $\boldsymbol{E}$ the total non-chemical energy. R in Eq. (5) is the specific gas constant. M is total species number. Only (M - 1) species mass fractions are solved, and the inert species, i.e., nitrogen, is calculated from $\sum_{m=1}^{M} Y_m = 1$. The source terms, S_{mass}, $\boldsymbol{S}_{mom}$, S_{energy}, and $S_{species,m}$, denote the inter-phase exchanges of mass, momentum, energy, and species, respectively. $\mathbf{T}$ represents the viscous stress tensor, while $\mathbf{j}$ is the diffusive heat flux. Moreover, $\boldsymbol{S}_m$ is the species mass flux. $\dot{\omega}_m$ and $\dot{\omega}_T$ are the net reaction rate of m-th species and combustion heat release rate, respectively.

As for the liquid phase, it is composed of a large number of spherical droplets, which are tracked by the Lagrangian method. The evolutions of mass, velocity, and temperature of individual fuel droplets are governed by

$$\frac{dm_d}{dt} = -\dot{m}_d \tag{6}$$

$$\frac{d\mathbf{u}_d}{dt} = \frac{\mathbf{F}_d}{m_d}, \tag{7}$$

$$c_{p,d} \frac{dT_d}{dt} = \frac{\dot{Q}_C + \dot{Q}_{lat}}{m_d} \tag{8}$$

where m_d is the droplet mass, $\mathbf{u}_d$ the droplet velocity vector, and T_d the droplet temperature. Moreover, the droplet evaporation rate $\dot{m}_d$ is calculated from

$$\dot{m}_d = \pi d Sh D_{ab} \rho_s \ln(1 + X_r), \tag{9}$$

where d is the droplet diameter, D_{ab} the vapor diffusivity in the gaseous mixture, and ρ_s the density on the droplet surface. $Sh = 2.0 + 0.6Re_d^{1/2}Sc^{1/3}$ is the Sherwood number, and Sc is the Schmidt number of the gas phase. The droplet Reynolds number, Re_d, is calculated based on the velocity difference between two phases, i.e., $Re_d \equiv \rho_d|\mathbf{u} - \mathbf{u_d}|/\mu$. ρ_d represents the droplet material density and μ is the dynamic viscosity of the gaseous mixture. In Eq. (9), $X_r \equiv (X_S - X_C)/(1 - X_S)$ is the concentration difference between the gas flow and droplet surface, scaled by that between the droplet surface and interior. X_C is the fuel species molar fraction in the surrounding gas, while X_S is the fuel species molar fraction at the droplet surface. $\mathbf{F}_d$ is the force acting on the droplets.

2.2 Numerical method

The governing equations for gas and droplet phases are solved by a hybrid Eulerian-Lagrangian solver *RYrhoCentralFoam*[7], which is developed based on *OpenFOAM*. The accuracies of the solver have been verified through extensive benchmark tests [14]. The results show that the *RYrhoCentralFoam* solver can accurately predict the response of fuel droplets to flows with shock waves and chemical reactions. More recently, this solver has been further applied to RDE modelling with gaseous and liquid fuels [15, 16]. Note that a two-step kerosene/air reaction mechanism [17] is used in the current study. The reliability of the two-step mechanism has been well confirmed in Ref [18, 19].

3 Results and discussion

Simulations were performed under Mach-5, 24-km operating conditions. Table 1 lists the main injection and outlet parameters adopted in this study. To investigate the engine size effects, four geometries (l_c*l_a) are adopted, i.e., G1(0.1*0.03 m), G2(0.2*0.06 m), G3(0.3*0.09 m), and G4(0.4*0.12 m). The grid size is 0.1 mm*0.1 mm. Furthermore, droplets size from 5 μm to 30 μm is taken into consideration. Specifically, in each geometry, four droplet sizes are simulated, i.e, 5 μm, 10 μm, 20 μm, and 30 μm. The equivalence ratio keeps around 1.1.

Table 1: Simulation conditions in this study.

Mach	Altitude /km	Recovery coefficient	Total pressure /MPa	Total temperature /K	Ambient pressure /Pa
5	24	0.54	0.93	1242	2930

Figure 1 shows the simulation results. Overall, most cases obtained self-sustained rotating detonation waves except for cases 3 and 4. In cases 3 and 4, a small engine size of 0.1*0.03 m is adopted and larger droplet diameters, i.e., 20 μm and 30 um. It can be found that small engine sizes and larger droplet diameters are unfavourable for the propagation of two-phase rotating detonation waves.

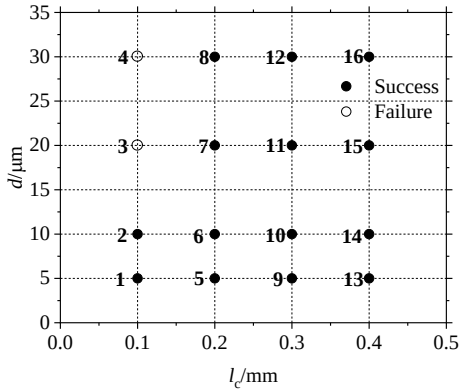

Figure 1: Propagation map vs. circumferential length l_c and droplet diameter d.

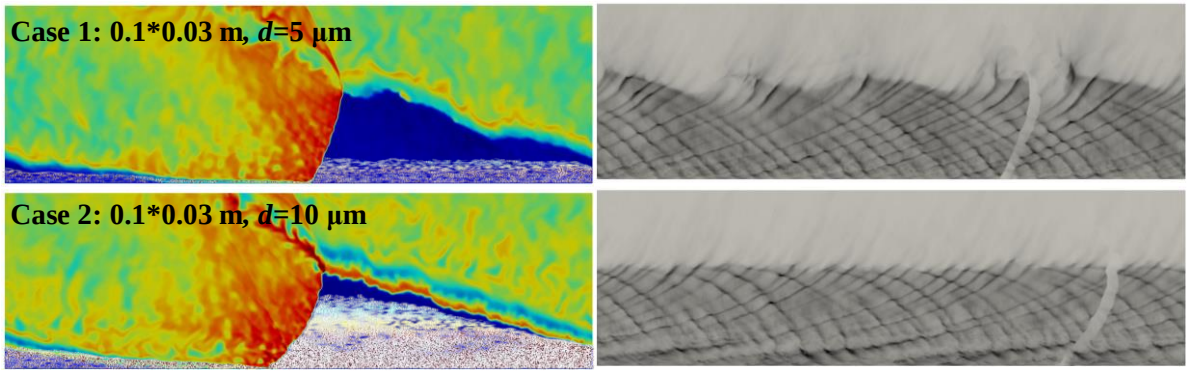

Figure 2: Temperature contour overlaid with droplet diameters and smoke foils of cases 1 and 2.

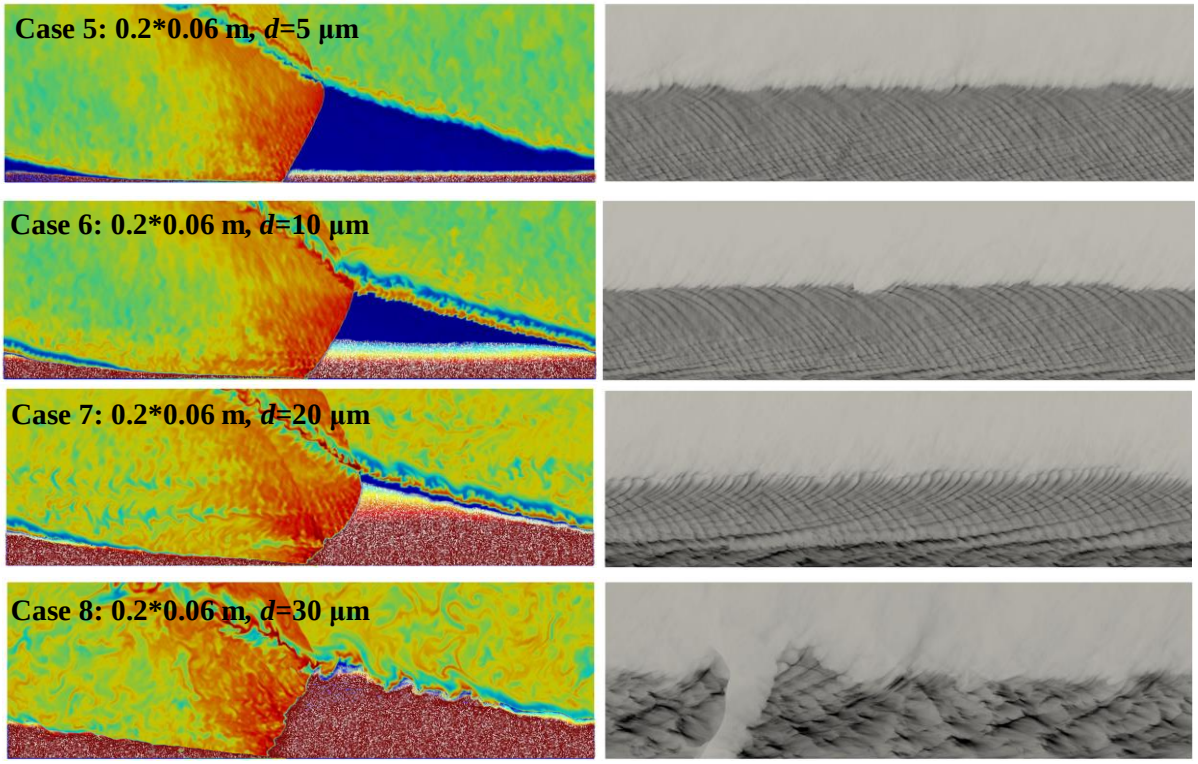

Figure 3: Temperature contour overlaid with droplet diameters and smoke foils of cases 5-8.

Figure 2 shows the temperature contours and smoke foils of cases 1 and 2. As can be seen, rotating detonation is ignited and succeeds in propagating with clear cellular traces. The smoke foils in these two cases are similar to the gaseous rotating detonations due to the small droplet size and high injection total temperatures. The droplets evaporate fast when injected in case 1 while almost reaching the detonation height in case 2.

Figure 3 shows the flow field of cases 5-8 where a larger engine size is adopted. It can be found that similar results in cases 1-2 are obtained in cases 5-6. However, the situation gets changed when d is further increased to 20 and 30 um. With increased engine size, rotating detonation is self-sustained at d=20 and d=30 um. Moreover, the flow field differs from the previous study in the degenerating of the detonation wave near the head end. A λ-shaped shock system is formed in the detonation front. The smoke foils near the head end are also indistinguishable, demonstrating significant two-phase detonation

features. When the droplet diameter increases to 30 um, the detonation front degenerates and the smoke foils are obscure.

Figure 4 shows the flow field of case 13-16 where a large engine size (0.4*0.12 m) are adopted. It can be found that the rotating detonation behaves more stably compared with cases 5-8. For example, the smoke foils in case 16 are divided into two layers. The lower layer is also obscure, the same as that in case 8. While the upper layer becomes clear with extensive cellular structures. The reason lies in the evaporation length of the droplets. The droplet absorbs heat from the hot gas and its temperature rises up to the boiling point. Once the droplet temperature reaches boiling point, evaporation becomes intense and can be fast consumed by the detonation front. Therefore, a sufficient long heating length for the droplets is the key to the two-phase rotating detonation propagation.

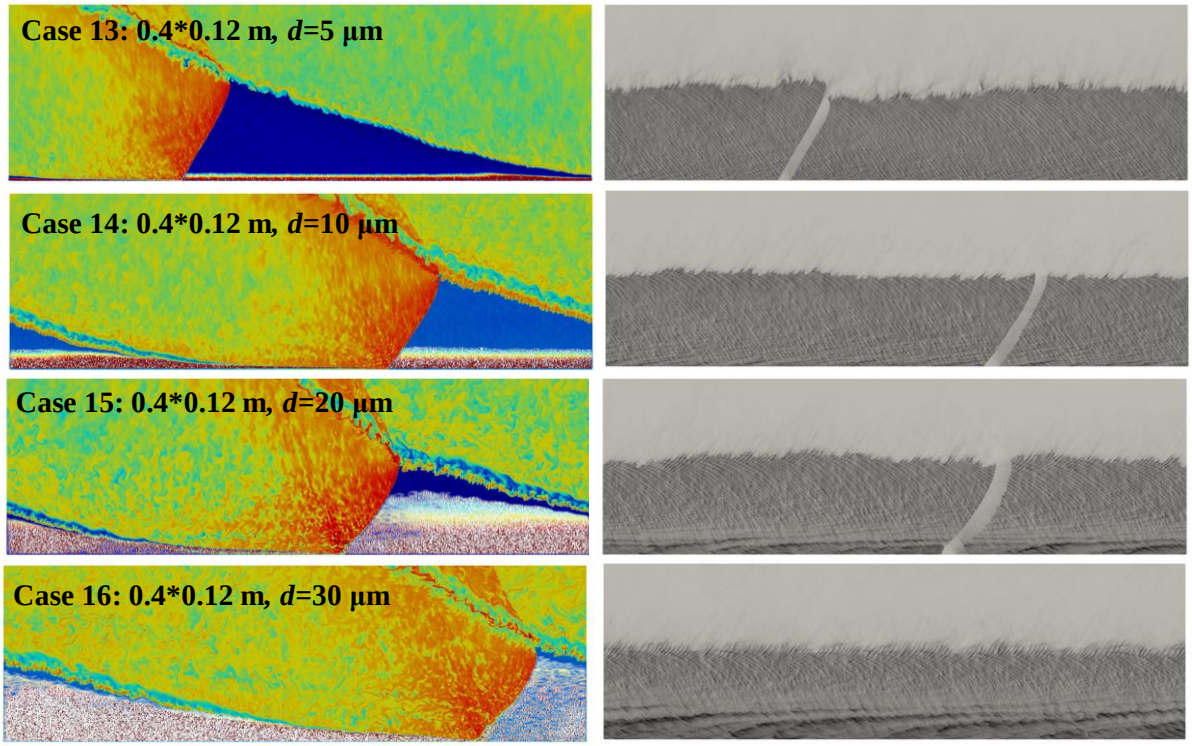

Figure 4: Temperature contour overlaid with droplet diameters and smoke foils of cases 13-16.

4 Conclusion

In this paper, numerical simulations were conducted to study the two-phase kerosene-air rotating detonation engines operating at the conditions of Mach 5 and 24 km. The Eulerian-Lagrangian method is adopted for two-phase modelling and a two-step chemistry is used for kerosene reaction. The engine sizes and droplet diameters are investigated.

The results found that small engine size and larger droplet diameter are unfavourable for the propagation of two-phase rotating detonation waves. When 5 μm and 10 μm droplets are adopted, the RDE behaves like gaseous rotating detonations with clear cellular structures. When the 20 μm and 30 μm droplets are adopted, the rotating detonation waves tend to be divided into two layers. The lower layer is indistinguishable while the upper layer becomes clear with extensive cellular structures. The results demonstrate large geometry size is crucial for the two-phase rotating detonation propagation and stability.

References

[1] V. Raman, S. Prakash, M. Gamba, Nonidealities in Rotating Detonation Engines, Annual Review of Fluid Mechanics, 55 (2023) 639-674.
[2] P. Wolanski, W. Balicki, W. Perkowski, A. Bilar, Experimental research of liquid-fueled continuously rotating detonation chamber, Shock Waves, 31 (2021) 807-812.
[3] H.L. Meng, Q. Xiao, W.K. Feng, M.L. Wu, X.P. Han, F. Wang, C.S. Weng, Q. Zheng, Air-breathing rotating detonation fueled by liquid kerosene in cavity-based annular combustor, Aerospace Science and Technology, 122 (2022) 1-11.
[4] W. Feng, Q. Zheng, Q. Xiao, H. Meng, X. Han, Q. Cao, H. Huang, B. Wu, H. Xu, C. Weng, Effects of cavity length on operating characteristics of a ramjet rotating detonation engine fueled by liquid kerosene, Fuel, 332 (2023).
[5] A.G. Martinez, S.D. Heister, Wave Structure of Heterogeneous Detonations in Rotating Detonation Rocket Engines, in: AIAA SCITECH 2022 Forum, San Diego, 2022.
[6] D. Lim, J. Humble, S.D. Heister, Experimental Testing of an RP-2-GOX Rotating Detonation Rocket Engine, in: AIAA Scitech 2020 Forum, Orlando, 2020.
[7] Z. Huang, M. Zhao, Y. Xu, G. Li, H. Zhang, Eulerian-Lagrangian modelling of detonative combustion in two-phase gas-droplet mixtures with OpenFOAM: Validations and verifications, Fuel, 286 (2021).
[8] M. Zhao, H. Zhang, Rotating detonative combustion in partially pre-vaporized dilute n-heptane sprays: Droplet size and equivalence ratio effects, Fuel, 304 (2021).
[9] S. Jin, C. Xu, H. Zheng, H. Zhang, Detailed chemistry modeling of rotating detonations with dilute n-heptane sprays and preheated air, Proceedings of the Combustion Institute, (2022).
[10] Q.Y. Meng, N.B. Zhao, H.W. Zhang, On the distributions of fuel droplets and in situ vapor in rotating detonation combustion with prevaporized n-heptane sprays, Phys Fluids, 33 (2021) 1-17.
[11] Z. Ren, L. Zheng, Numerical study on rotating detonation stability in two-phase kerosene-air mixture, Combustion and Flame, 231 (2021).
[12] F. Wang, C.S. Weng, Numerical research on two-phase kerosene/air rotating detonation engines, Acta Astronautica, 192 (2022) 199-209.
[13] C.T. Crowe, J.D. Schwarzkopf, M. Sommerfeld, Y. Tsuji, Multiphase flow with droplets and particles, 2011.
[14] Y. Xu, H. Zhang, Pulsating propagation and extinction of hydrogen detonations in ultrafine water sprays, Combustion and Flame, 241 (2022).
[15] M. Zhao, Z. Ren, H. Zhang, Pulsating detonative combustion in n-heptane/air mixtures under off-stoichiometric conditions, Combustion and Flame, 226 (2021) 285-301.
[16] Q.Y. Meng, M.J. Zhao, H.T. Zheng, H.W. Zhang, Eulerian-Lagrangian modelling of rotating detonative combustion in partially pre-vaporized n-heptane sprays with hydrogen addition, Fuel, 290 (2021) 1-17.
[17] B. Franzelli, E. Riber, M. Sanjosé, T. Poinsot, A two-step chemical scheme for kerosene–air premixed flames, Combustion and Flame, 157 (2010) 1364-1373.
[18] F. Wang, C. Weng, Effects of Divergence Inlet on Kerosene/Air Rotating Detonation Engines, AIAA Journal, 60 (2022) 4578-4600.
[19] F. Wang, C. Weng, Preliminary Criterion for Positive Total Pressure Gain in Kerosene/Air Rotating Detonation Combustor, AIAA Journal, 60 (2022) 6548-6556.